

An Integrated Approach to Modeling and Mitigating SOFC Failure
(Agreement No. DE-AC26-02NT41571)

Monthly Project Highlight Report

for the period of

July 1, 2003 – July 31, 2003

to

Travis R. Shultz
National Energy Technology Laboratory

From

PI: Jianmin Qu,
Co-PIs: Andrei Fedorov and Comas Haynes

School of Mechanical Engineering
Georgia Institute of Technology
801 Ferst Drive, N.W.
Atlanta, Georgia 30332-0405
Phone: 404-894-5687
FAX: 404-894-0186
E-Mail: jianmin.qu@me.gatech.edu

July 31, 2003

Agreement No.: DE-AC26-02NT41571

Reporting Period: – July 1, 2003 – July 31, 2003

Summary of Activities

Major activities of this month include

- Developed a model for simulating thermal spalling failure during steady-state operation.
- Established the analogy between fuel cells and heat exchangers.
- Modeled a realistic geometry of the monolith SOFC with the flow channels not included within the electrodes.
- Studied the effect of radiation on the temperature fields of the modified, more realistic monolith SOFC geometry

Technical Highlights

Task 1: Fracture Mechanics Modeling

1.2 Model spalling phenomenon and thermal expansion induced stress during thermal transients and shock.

During the start-up or steady-state operation, there is typically a temperature gradient along the air channel. Such non-uniform temperature distribution causes stresses in the P-E-N structure. When such thermally induced stresses are sufficiently high, mechanical damage (spalling or microcracking) may occur in the P-E-N structure. Intuitively, it is conceivable that the higher the temperature gradient induces higher stresses. Therefore, to model and mitigate spalling/microcracking, accurate prediction of temperature distribution and the corresponding stresses is very critical.

During steady state operation of solid oxide fuel cells, air flows in the air channels over the cathode. To improve the overall efficiency of the system, it would be more cost effective to pump ambient temperature air into the air channel inlet. However, this is not practical because the cell stack is very hot ($\sim 800^{\circ}\text{C}$) during operation. Cold air at the air channel inlet will result in large temperature gradient, causing thermal spalling of the cathode. To avoid such damage to the cathode, air must be pre-heated, which encumbers additional capital costs for the supplemental hardware and added size. In addition to the inlet air temperature, the air flow speed is another critical parameter that may affect the thermal stress in the cathode. It is therefore advantageous to develop a model for predicting the minimum air temperature at the inlet and the optimal flow speed without causing spalling damage to the cathode.

In this report, we develop a methodology and associated algorithms that establish the relationship between airflow (temperature and flow speed) and the thermal shock induced stress within the cathode. This model can be used in predicting locations of failure within the P-E-N. Then the required inlet air temperature and velocity can be

optimized for safe operation of the SOFC stack without compromising the efficiency of the overall SOFC system.

To illustrate the model development, a three-layer P-E-N structure was considered, see Fig. 1.1. The air flows over the cathode. The problem was constructed as a steady-state, forced convection problem. Convection is the heating or cooling effect experienced by a solid as a fluid flows over it. Forced convection comes about by external means such as a fan or pump. Newton's law of cooling states the heat loss of an object is proportional to the convection coefficient and the difference between the temperature of the surface and the bulk temperature of the fluid as shown in equation 1.1.

$$\dot{Q}_{convection} = hA(T_{surface} - T_{bulk}) \quad (1.1)$$

The convection coefficient, h , may vary along the length of the surface and is dependant on the velocity of the air flow, geometry, and fluid thermophysical properties. Accurate determination of the convection coefficient for the specific geometric arrangement requires experimentation, but the value can be approximated using available correlations (see Appendix A). It should be noted that for this analysis the convection was calculated for laminar flow.

Further assumptions were that the problem is steady-state and a given temperature differential is prescribed between the inlet and outlet air temperatures. The variation of temperature along the air flow was considered to be linear for simplicity. Finally, it was assumed that during the operation, the fuel cell maintained a constant 800°C temperature along the bottom edge of the anode and that adiabatic conditions existed at either end physically corresponding to perfect thermal insulation. Figure 1.1 shows the boundary conditions used for the problem and the thermal and mechanical properties of the PEN structure are listed in Table 1.1.

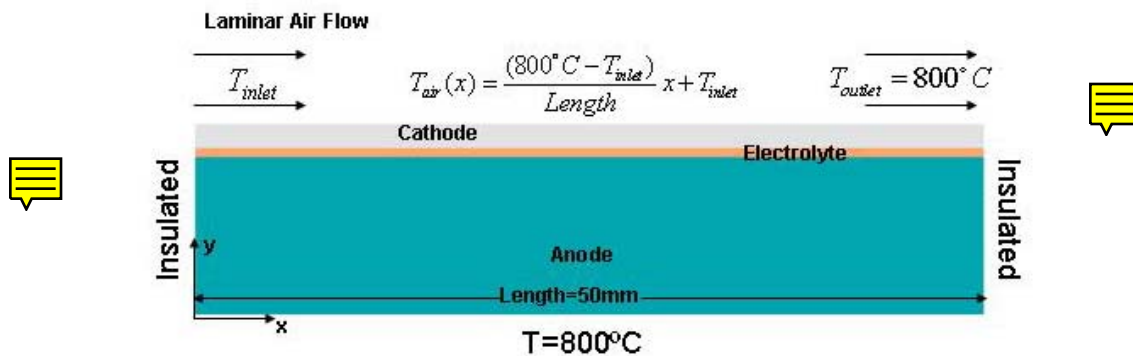


Figure 1.1: Boundary Conditions of Thermal Model

The structural model was considered pinned at the origin and set on rollers in the y -direction at $x = 0$. This means that expansion was not constrained in the x or y directions. For each analysis the coefficient of thermal expansion (CTE) reference temperatures was 600°C. The reference temperature of the CTE is where the model is considered to be free of residual stresses.

Table 1.1 Properties used in Finite Element Analysis

Materials	Young's Modulus (GPa)	Poisson's Ratio	CTE (10-6/°C)	Thermal Conductivity (W/mK)	Layer Thickness (mm)
Cathode (LSM+YSZ)	96	0.3	10.56	1.86	.075
Electrolyte (YSZ)	200	0.3	10.56	2.16	.015
Anode (Ni+YSZ)	96	0.3	12.22	5.84	.500

Fem Model:

A two dimensional model was constructed and analyzed using the ANSYS 7.0 software. The thermal and structural analysis was combined using an indirect coupled method. Procedurally this means the thermal analysis was solved first and the resulting temperature gradient was input as a boundary condition for the structural model.

The thermal model used Plane77 elements, which are 8node thermal elements, with temperature as the one degree of freedom. After the thermal analysis the elements were converted to Plane82, a structural 8node element with degrees of freedom in the *x*, *y*, and *z* directions. The model was considered to be under plane strain.

A mapped mesh was used and the following parameters were used to set the element size as shown in Table 1.2. A total of 18,400 elements were used.

Table 1.2 Mesh Parameters

PEN Location	Size Ratio	Actual Size (50mm x 0.59 mm model)
Length (x-dir)	Length/800	.0625 mm
Anode (y-dir)	Anode height /16	.03125 mm
Electrolyte (y-dir)	Electrolyte Height/3	.005 mm
Cathode (y-dir)	Cathode Height/4	.01875 mm

Results:

Initially only the effect of flow velocity was examined on the composite layers. This was done by varying the velocity in the calculation of the convection coefficient. Figure 1.3 shows a plot of the temperature across the upper edge of the cathode. It is at the top edge of the cathode that the cooling effect of the air flow is most pronounced, because the heat transfer coefficient is highest at the leading edge and air is at its coolest state. It can be seen from the plot, the temperature began to approach 800°C at approximately 5mm into the PEN structure.

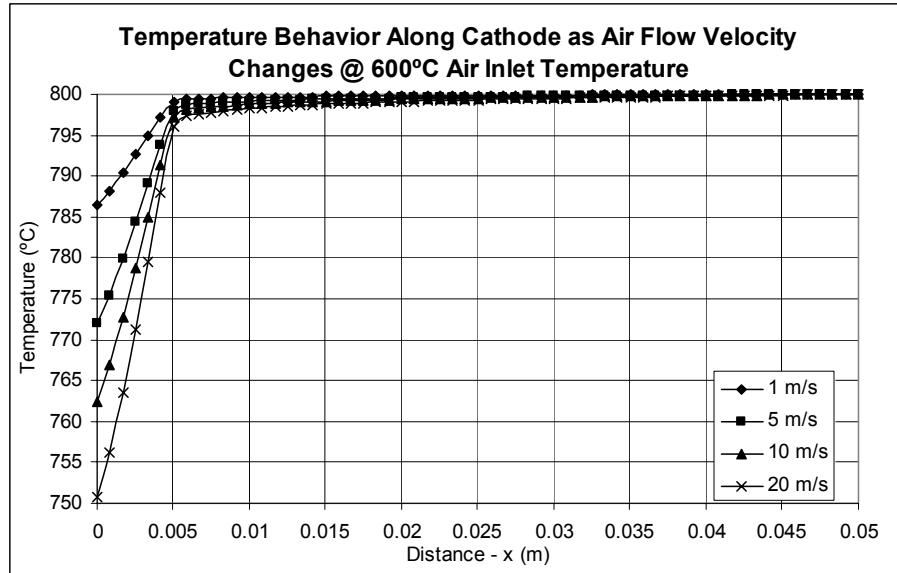


Figure 1.3: Temperature Behavior as function of air velocity

In the next step, we held the velocity constant and changed the value of the air inlet temperature. Examination of Figure 1.4 shows much the same behavior as seen in Figure 1.3. As expected, the colder is air the greater is the temperature gradient.

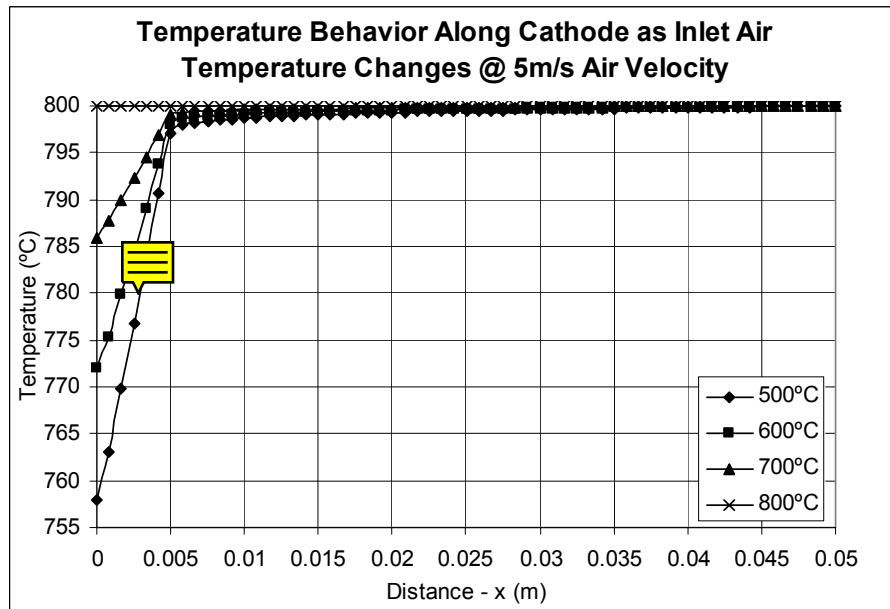


Figure 1.4: Temperature Behavior as related to inlet temperature

According to the theory of thermal elasticity, the stresses generated by non-uniform temperature field are proportional to the temperature (spatial) gradient. Since the largest temperature gradient occurred near the inlet, the structural analysis focused on this area. Even though thermal mismatch still occurred, stress behavior in areas of uniform temperature will also be uniform in the x-direction. It is in areas of non-uniform temperature that the highest stresses will occur in the cathode. It is then at these locations possible failure could occur. Figures 1.5 and 1.6 are contour plots from ANSYS showing the temperature and sigma x fields in the region of interest.

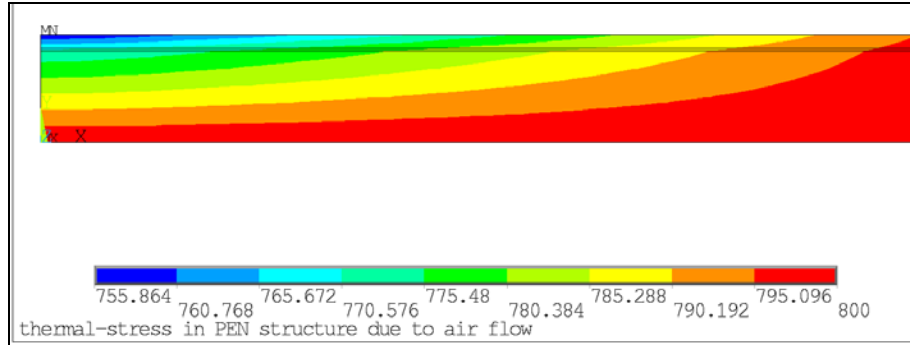


Figure 1.6: Temperature (°C) variation for @ 600°C inlet and 15m/s velocity

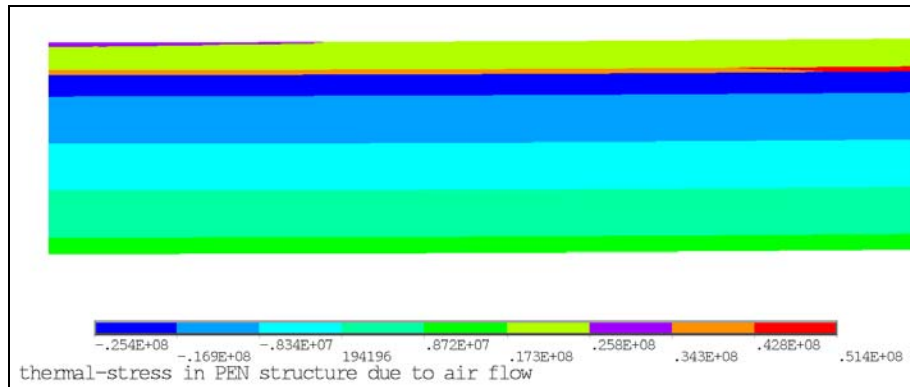


Figure 1.7: Stress in x-direction (Pa) variation for @ 600°C inlet and 15m/s velocity

Since it can be seen from these plots that the highest stress in the cathode occurs near the air inlet, this becomes the place failure is most likely to occur. When the maximum stress in the cathode is plotted against the inlet air temperature and the velocity the relationship appears to be linear. It is only at 1 m/s that nonlinear behavior can be seen. The plots are shown below in Figures 1.8 and 1.9.

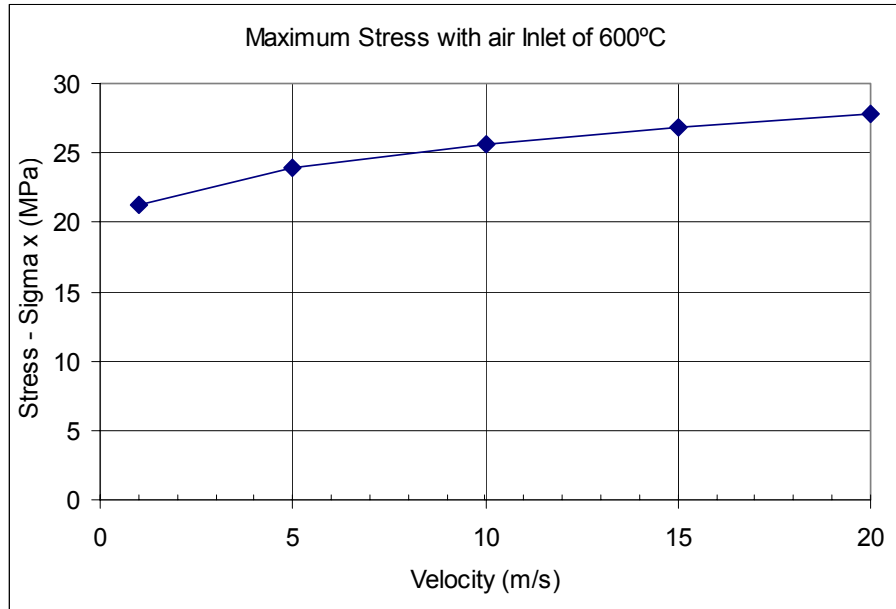


Figure 1.8: Stress and Velocity

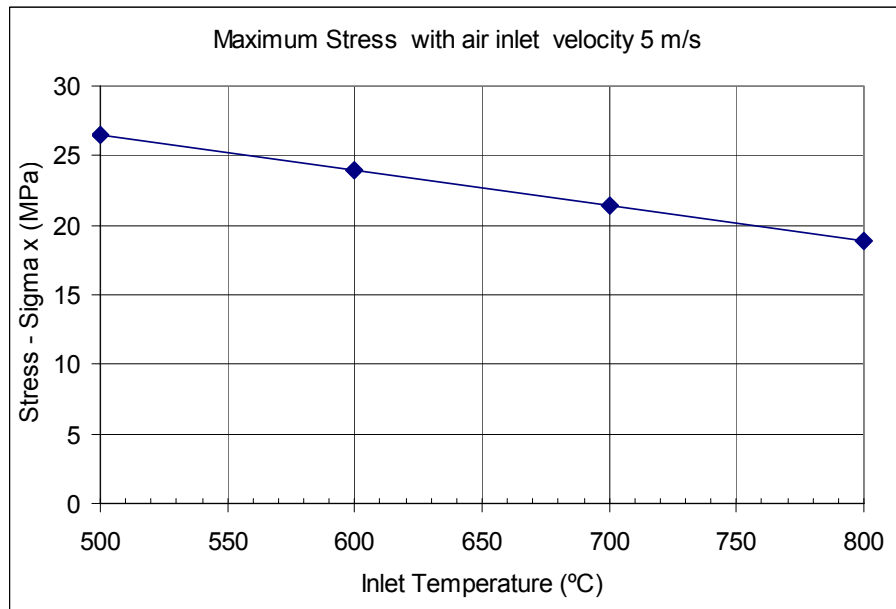


Figure 1.8: Stress and Temperature

It is seen from these plots that the thermal shock induced stress increases for increasing air flow speed. The thermal stress also increases with decreasing inlet air temperature, as expected. The model developed here provides a tool for designing a cell stack with optimal operating conditions (inlet air temperature and flow speed) without inducing thermal spalling failure of the cathode near the air inlet.

Task 2: Electrochemical Modeling

2.1 Utilize/adapt existing electrochemical models, and develop enhancements necessary to achieve the project objectives and to advance the state-of-the-art.

As a possible enhancement to the state-of-the-art of fuel cell modeling and design, the following set of analogs has been established between fuel cells and heat exchangers. The end-goal is to glean principles from the mature areas of heat exchanger design and characterization into similar areas within the maturing field of fuel cells simulation. Focused attention is given to the concept of electrochemical pinch points as a supplement to traditional fuel cell parameters.

Analogies Between Fuel Cells and Heat Exchangers

Fuel cells are direct energy converters that continuously and electrochemically convert chemical energy into electricity. Like their galvanic cell counterparts (i.e., batteries), their fundamental components are positive and negative electrodes (cathode and anode, respectively), and an ion-conducting electrolyte between the electrodes. Unlike batteries, fuel cells are theoretically invariant with time, because the reactants and products are within the flows entering and exiting these open systems. Figure 2.1 illustrates the principles of fuel cell operation.

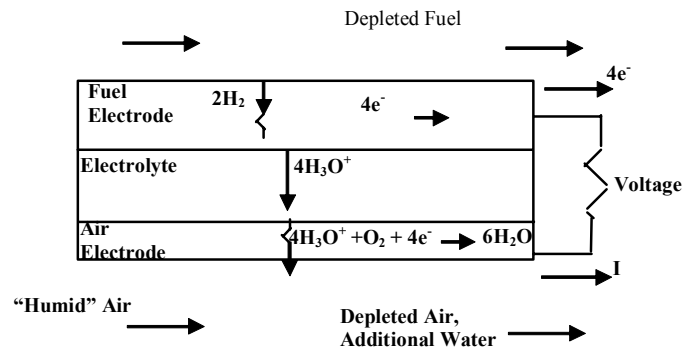


Figure 2.1(a): Cation-conducting fuel cell (PEFC with electro-osmotic drag ratio of 1 $\text{H}_2\text{O}: 1 \text{H}^+$)

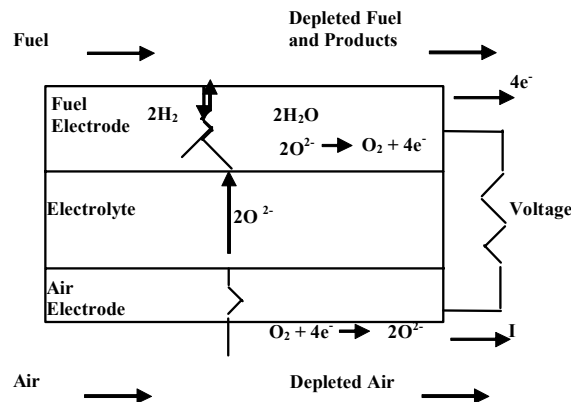


Figure 2.1(b): Anion-conducting fuel cell (solid oxide example)

The primary reactants used are hydrogen and oxygen, with water as the product. Lower temperature fuel cells are predominantly cationic conductors (e.g., polymer electrolyte membrane and phosphoric acid fuel cells); higher temperature fuel cells are predominantly anionic conducting (e.g., molten carbonate and solid oxide fuel cells). Fuel cells, in general, are found to have significant parallels with heat exchangers.

Analogous transport phenomena via potential differences

Heat exchangers foster thermal energy transport (heat) as a result of thermal potential differences ($T_h - T_c$) between streams; similarly, fuel cells foster charge transport (current) as a result of electrochemical/electrical potential differences ($\mathcal{E} - V_{\text{cell}}$) between the reactants streams' Nernst potential and the actual cell potential. Elaborating upon this latter point, the chemical Gibbs free energy release of hydrogen oxidation is ideally converted to electricity, wherein the thermodynamic voltage across cell electrodes is termed the Nernst potential. Actual fuel cell voltages are less than corresponding Nernst potentials due to electrochemical inefficiencies. The differences between Nernst and actual cell potential, along the fuel cell, govern charge transport as follows.

$$i = \frac{E - V_{\text{operate}}}{R_{\text{electrode,cathode}} + R_{\text{conduction,ohmic}} + R_{\text{electrode,anode}}} \quad (2.1)$$

The resistances within the denominator are reflective of electrode polarizations and internal (ohmic) resistance. These three resistances, in series, are next explained.

Analogous resistances

The air electrode, or cathode, is the site of electrochemical reduction reaction(s); mass and charge transfer barriers therein lead to polarization (i.e., departure from thermodynamic electrode potential). The fuel electrode, or anode, is the site of electrochemical oxidation reaction(s); likewise, mass and charge transfer resistances lead to polarization. Additionally the cell's material resistivities result in ohmic losses. Figure 2.2 illustrates these series electrochemical resistances.

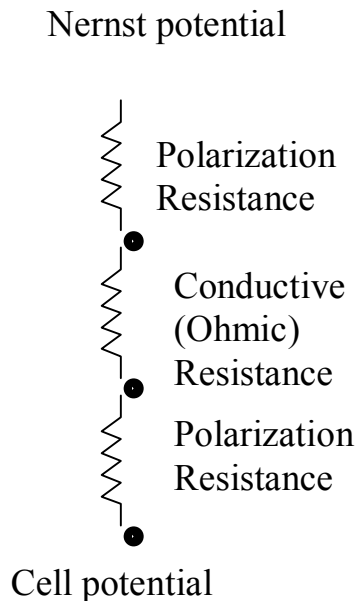


Figure 2.2: Electrochemical resistances to current and power generation

Heat exchangers have analogous resistances. A heat exchanger, with the equivalent resistances, is illustrated in Figure 2.3. Just as an electrode is characterized by its polarization during charge transport, the convective resistance that occurs during thermal transport characterizes each fluid stream in a heat exchanger. The electrolyte is the primary electrochemical conductive resistance. The vessel separating the hot and cold streams of a heat exchanger likewise presents a thermal conductive resistance.

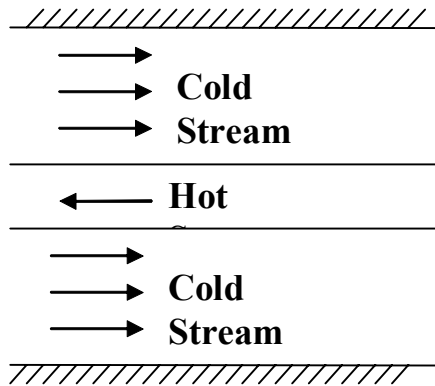


Figure 2.3 (a): Heat exchanger axial cross section

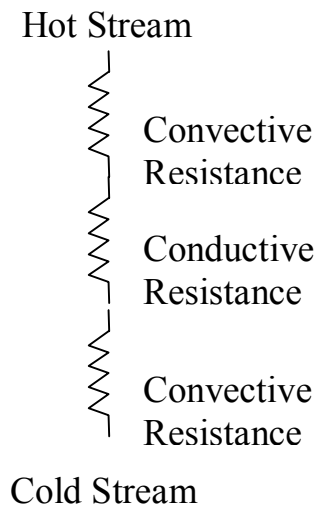


Figure 2.3 (b): Thermal resistances

Summarizing the analogies between fuel cell and heat exchanger potential differences and resistances, one can compare Eqn. (2.1) to the following Eqn. (2.2) that characterizes heat exchanger heat transfer¹.

$$q = \frac{T_h - T_c}{R_{\text{convectionhot-stream}} + R_{\text{conductionthermal}} + R_{\text{convectioncold-stream}}} \quad (2.2)$$

Analogous regions of transport phenomena

Another similarity between fuel cells and heat exchangers is the performance and cost impact of designing the regions of active transport phenomena. Fuel cell electroactive area is the region over which electrochemical reactions cause transport phenomenon current; power is the energy-in-transit produced. Heat exchangers have an analogous region over which stream temperature differences cause thermal transport; heat is the energy-in-transit produced. This is the heat exchanger's active area (i.e., the "A" factor in the commonly referenced "UA" metric). Fuel cells are given load demands for both current and power. Larger electroactive areas allow for these demands to be met at higher efficiencies (i.e., larger cell potentials). Likewise, larger "UA" allotments allow for heat exchangers to service a given heat load with improved thermal contact between the streams. A trade-off, however, is the required capital investment. Both the electroactive area and the UA are major determiners of cost in fuel cells and heat exchangers, respectively; hence, the design methodologies that minimize materials investments within heat exchanger design may be translatable into cost-saving measures in fuel cells design. Another trade-off is that power density may lessen at larger electroactive areas due to decreased current density, yet large power densities are critical to mobile applications, which is the largest potential market for fuel cell systems.

Analogous capacity rates

Finally, heat exchanger and fuel cell reactant streams have analogous capacity rates. Heat exchanger flows are characterized by heat capacity rates. Similarly, fuel cells may have electrochemical capacity rates defined.

$$\dot{C}_{\text{stream}} = \frac{\dot{Q}}{dT} \quad (2.3a)$$

$$\dot{E}_{\text{streams}} = \frac{i}{dE} \quad (2.4)$$

Eqns. (2.3a) and (2.4) are definitions given for heat and electrochemical capacity rates in heat exchangers and fuel cells, respectively. The numerator of each identifies the objective transport phenomenon, and the denominators indicate the corresponding change in the relevant potential property. Qualitatively, heat capacity rate measures the impact of

¹ Both electrochemical and thermal conduction resistances include any contact resistances between fuel cell layers and heat exchanger walls, respectively.

thermal transport upon stream thermal potential. Likewise, the defined electrochemical capacity rate measures the impact of charge transport upon streams' Nernst potential².

Consider the factors that govern Nernst potential.

$$nFE = -\Delta G_{H_2 \rightarrow H_2O}^o - R_u T \ln \left[\frac{P_{H_2O}}{P_{H_2} P_{O_2}^{1/2}} \right] \quad (2.5)$$

Eqn. (2.5) relates Nernst potential to the electrochemical oxidation of hydrogen³. Notice the dependence of Nernst potential upon constituent partial pressures. This dependence is pivotal to the analog of an electrochemical capacity rate.

Neglecting head loss, partial pressures depend explicitly upon constituent mole fractions along the cell. These mole fractions in turn depend upon the molar flows within the stream. The molar flows of electroactive species change as a result of current generation along the cell axis. This change in constituents is quantified via Faraday's Law.

$$\Delta \dot{n}_j = \frac{V_j i}{nF} \quad (2.6)$$

Faraday's Law is an electrochemical statement of mass conservation, stoichiometrically relating changes in reaction participants to current generation. *Current* thus affects electroactive species flowrates, which affect mole fractions and partial pressures, ultimately impacting *Nernst* potential. This is analogous to the impact of *heat transfer* upon stream *thermal* potential. The capacity rate analogy has a final nuance.

Presuming sensible heating, a stream's heat capacity rate may be further defined as the product of mass flow and specific heat at constant pressure.

$$\dot{C}_{stream} = \dot{m} c_p \quad (2.3b)$$

Eqns. (2.3) reveal that a stream's temperature change due to heat is diminished by a larger mass flowrate (extensive parameter) and larger specific heats associated with its constituents (intensive parameters). Likewise, given an amount of current generation, the change in Nernst potential is dampened by larger molar flows (extensive parameter) and higher partial pressures (intensive parameters) of the electroactive species.

General and Specific Analogies between Fuel Cells and Heat Exchangers

Table 1 summarizes the analogs discussed of fuel cells in relation to heat exchangers. It includes fundamental characteristics of each technology. Fuel cells have thus been generally related to heat exchangers, yet there is a more specific similarity between fuel cells and evaporative heat exchangers.

Table 2.1: Parallels Between Heat Exchangers and Fuel Cells

²A heat capacity rate must be defined for each heat exchanger stream; however, the electrochemical capacity rate is inclusive of both fuel and oxidant streams, since both factor into the resolution of Nernst potential. *Typically, however, the fuel stream is the dominant influence.*

³ Primary reaction for fuel cell operation; all constituents are presumed to behave as ideal gases.

	Heat Exchanger	Fuel Cell
<i>Transport Phenomenon</i>	Heat	Current
<i>Driving Potential</i>	$T_h - T_c$	$\mathcal{E} - V_{\text{cell}}$
<i>Resistances</i>	Conductive; Convective	Conductive (ohmic); Polarization
<i>Region of Transport Phenomenon</i>	Heat Exchange Area	Electroactive Area
<i>Capacity Rate</i>	Heat Capacity Rate	Electrochemical Capacity Rate

Consider the usage of an evaporator as the heat exchanger example given in Figure 2.4(a). Neglecting head loss, an evaporator with a saturated conditions cold stream has the temperature profiles shown. Most fuel cells have sufficiently conductive electrodes, such that their operating voltage may be considered uniform, thus resulting in a Dirichlet boundary condition. Axial Nernst potential decreases along the fuel cell because of reactants consumption. The potential profiles shown in Fig. 2.4(b) thus manifest. The similarity between the temperature and voltage profiles in Fig. 4 is thus a final testament of the analogies between fuel cells and (evaporative) heat exchangers.

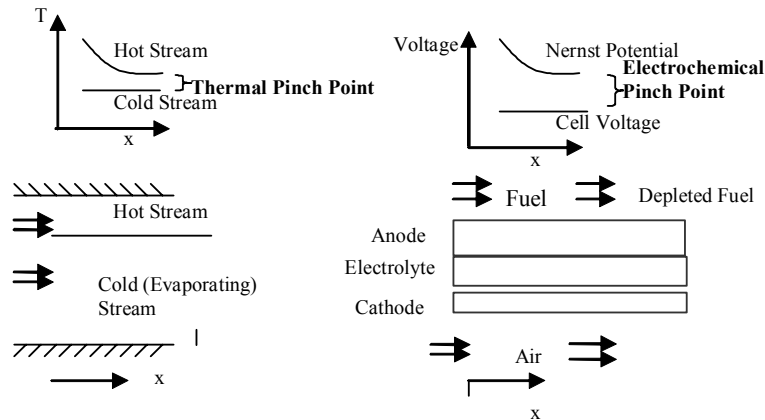


Fig. 2.4(a): Illustration of Thermal Pinch Point

Fig. 2.4(b): Illustration of Electrochemical Pinch Point

Electrochemical Pinch Points: A Complement to Traditional Fuel Cell Parameters
 Along with the need for continued research and development in enabling technology areas such as electrochemistry, materials science and fuel processing, the dominant barrier to fuel cells impacting the power generation market is their cost. Fuel cell systems cost on the order of thousands of dollars per kilowatt capacity, while heat engines cost

tens (cars) to hundreds (power plants) of dollars per kilowatt. Extending the pinch point concept from heat exchangers to fuel cells may decrease cell stack costs.

Referring again to Fig. 2.4, the pinch point concept is illustrated. Conventionally, a pinch point is the lowest allowable temperature difference in the design of a heat exchanger network (HEN). For simplicity, consider the single hot and cold stream evaporator network shown in Fig. 2.4(a). A pinch point that is too high leads to exorbitant irreversibilities due to heat transfer across relatively large temperature differences. A pinch point that is too low, however, results in excessively small heat flux along the heat exchanger. Both scenarios can be costly. Large pinch points result in larger operating costs due to increased *exergy* destruction within the heat exchanger. Small pinch points would, however, incur greater capital costs due to the needed increase in conductance (i.e., UA) for a given heat load. Pinch point methodologies successfully consider the trade-offs between capital and operating costs, and they have been used extensively to optimize heat exchangers. Consider the establishment of *electrochemical* “pinch points” (i.e., lowest allowable differences between Nernst potentials and cell operating voltage) which occur at the fuel cells’ trailing edges (Fig. 2.4b). Specifically, higher operating voltages would foster larger cell stack efficiencies. Such an operating potential, however, would require significantly lower current and power densities (analogous to heat flux) because of the smaller electrochemical pinch point. Specifically, the axial differences between Nernst and cell potentials would be significantly lower. For cell current to remain unchanged, then, the electroactive area of the fuel cell would have to be increased. Quantitative examples are next discussed.

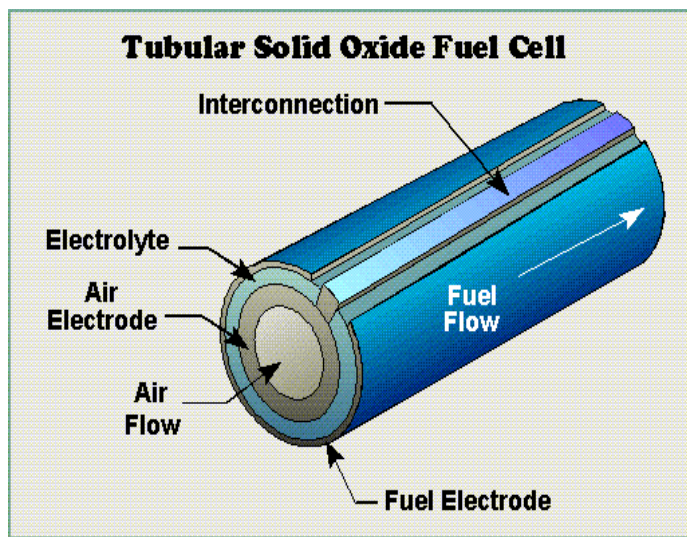


Figure 2.5: Isometric view of a SiemensWestinghouse TSOFC

Figure 2.5 illustrates a SiemensWestinghouse tubular SOFC (TSOFC). The cathode, or air electrode, is made of strontium-doped lanthanum manganite. The electrolyte is composed of yttria-stabilized zirconia. The anode, or fuel electrode, is made of a nickel-zirconia cermet. Current is extracted from an interconnect material of doped lanthanum chromite. Nickel felt contact padding (not shown) serves as the means of connecting individual cells into arrays or “stacks”. The cells are 2.2 cm (0.86 inches) in

outer diameter and 1.5 meters (59 inches) in length; electroactive area is 834 cm^2 . The design has been tested stringently and proven reliable, as exemplified in its continued record for fuel cell operating hours.

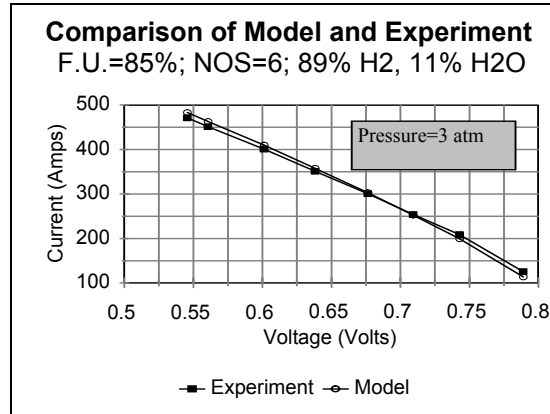


Figure 2.6a: Validation of model (3 atm)

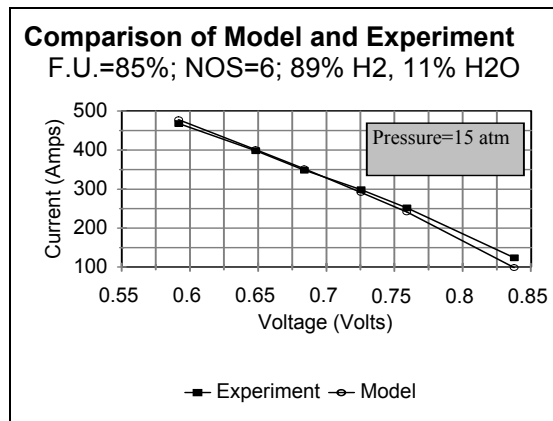


Figure 2.6b: Validation of model (15 atm)

The cell's electrochemistry was successfully simulated, as illustrated in Fig. 2.6⁴. Model predictions and experimental data were consistently within 3-5%, and the model was used to begin analyzing the effect of pinch point selection.

A conventional TSOFC (i.e., having the cited dimensions) was simulated under the various operating conditions of Fig. 2.6a. Prescribing the reactant flows and current generated by the conventional cell, the cell's length was then increased so that electroactive area increased proportionately.

⁴ I-V curves are shown instead of V-I curves, because voltage is the independent variable in the cell model.

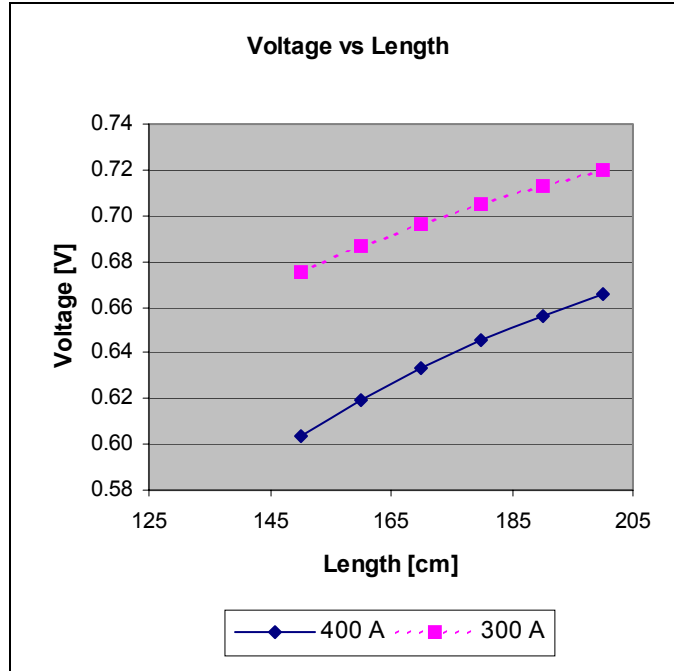


Fig. 2.7: Impact of increased electroactive area on cell voltage

Two scenarios are shown in Fig. 2.7, wherein the current demands of a TSOFC are 300A and 400A. Increasing the cell length (hence electroactive area) resulted in lower (area-specific) current densities; hence, operating voltage increased due to diminished electrochemical losses⁵. Note that cell power and efficiency are directly proportional to operating voltage. As an example then, the 400A rated cell would increase both in power and efficiency by more than ten percent over the given domain. *Is this increase in performance worth the additional capital costs associated with the one-third increase in electroactive area?* Again this is a benefit of extending the pinch point concept from heat exchangers to fuel cells.

⁵ Electrochemical losses are proportional to current density.

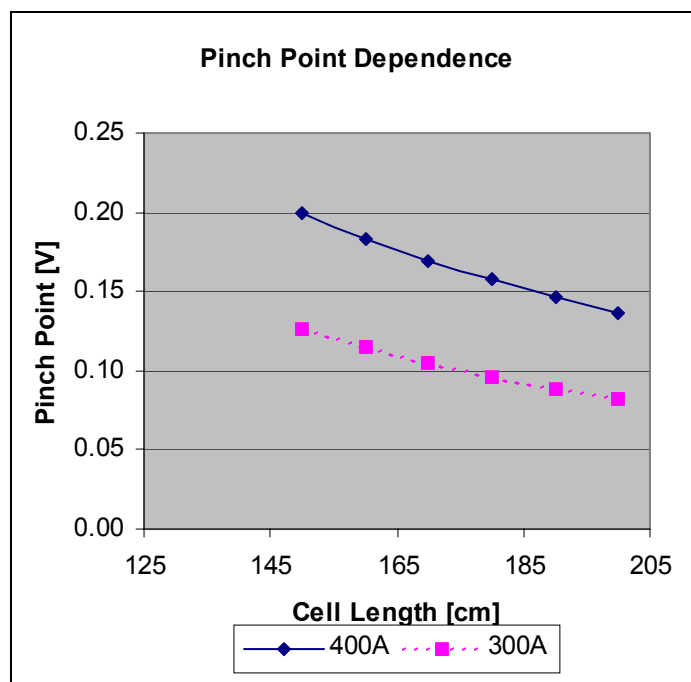


Fig. 2.8: Impact of increased electroactive area on resultant pinch points

Figure 2.8 corresponds to Fig. 2.7, except the defined electrochemical pinch points (i.e., the difference between the end-of-cell Nernst potential and operating voltage) are now graphed in place of cell voltage. The increases in cell voltage result in smaller electrochemical pinch points. The optimization of allotted electroactive area may now be cast as a decision about the optimal electrochemical pinch point, just as the optimization of heat exchanger UA (often focusing upon area A) may be cast as a decision about the optimal thermal pinch point (i.e., finding the best cost trade-off between manufacturing and operating costs). **There are numerous pinch point analyses methods that may thus be bridged from heat exchangers to fuel cells.**

Electrochemical pinch points may also serve as a complementary design parameter for the conventional measures cell potential and fuel utilization. Typically fuel cells designers prescribe a design voltage for a cell of prescribed current (density). The challenge is that in such a scenario operating voltage cannot be independently prescribed; yet, it is dependent upon reactant streams' Nernst potentials. Specifically, a cell's potential cannot be greater than the Nernst potential at the end of the cell. Depending on a variety of factors such as cell temperature, fuel/oxidant stream purity, and reactant utilization, Nernst potentials vary significantly. The designer must then investigate extensively to ensure that an aggressive operative voltage is feasible. Utilizing electrochemical pinch points alleviates this task, because Nernst potential is already an inherent part of the design point selection. Another conventional measure that may be supplemented by the concept of electrochemical pinch points is fuel utilization. As the name implies, fuel utilization is the fraction or percentage of supplied fuel that is *electrochemically* consumed. It is an important parameter, since fuel cells do not utilize all of the reactants fed to them. Simple (i.e., single-pass, hydrogen feed) cells are well characterized by fuel utilization, but the term can be arbitrary when considering more complex cells such as SOFCs.

As alluded to, SOFCs can utilize carbon monoxide (CO) within the fuel stream. This is especially advantageous, since hydrocarbon fuel processing typically produces CO as a by-product to hydrogen. Conventionally then, SOFC fuel utilization is calculated via the following.

$$u = \frac{(\dot{n}_{H_2} + \dot{n}_{CO})_{inlet, cell} - (\dot{n}_{H_2} + \dot{n}_{CO})_{exit, cell}}{(\dot{n}_{H_2} + \dot{n}_{CO})_{inlet, cell}} \quad (2.7)$$

The first point of uncertainty with regard to the defined fuel utilization is whether or not CO becomes oxidized electrochemically or via the shift reaction⁶; although shift is understood to be more prevalent, either reaction is feasible. This query is especially important, since the electrochemical oxidation of CO has substantially different characteristics and results than does the electrochemical oxidation of hydrogen, *and fuel utilization inherently refers to electrochemical fuel consumption.*

Consider two fuel cell scenarios wherein “X” amount of moles of reformat CO become CO₂, in addition to the electrochemical oxidation of “Y” moles of hydrogen. In the first case, the conversion of CO is by way of shift to hydrogen; in the latter case the conversion of CO includes a significant amount of both shift and electrochemical oxidation⁷. Despite the same calculated value for fuel utilization, the cell performances will be dissimilar. This thus causes a concern about whether cell performance is a true *function* of fuel utilization, since by mathematical definition, a standard function of x, f(x), should have one and only one value for each value x_i. Another point of ambiguity regarding fuel utilization arises when there is fuel stream recirculation.

As mentioned previously, SOFCs have the ability to internally reform hydrocarbon fuel into hydrogen-rich synthesis gas. This means fuel processing is done *in situ*. Although fuel processing occurs within the stack, it typically does not take place over the fuel electrode (i.e., no *direct* internal reformation). Such an arrangement would heighten the likelihood of carbon deposition (coking) on the anode. Additionally, electroactive anode surface area is valuable. In a direct internal reformation scenario, the cells’ leading edge electroactive area could be underutilized due to “syn gas” not yet being formed. Finally, direct internal reformation could produce unwanted “cold spots” on the fuel cell due to the reaction’s endothermic nature. The prevalent form of internal reformation is thus *indirect* internal reformation (IIR) wherein fuel processing occurs within the stack, but in compartments adjacent to the fuel cells.



⁶ Shift reaction: $CO + H_2O \rightarrow H_2 + CO_2$

⁷ The constituency of the reformat feed and electrode microstructure significantly influence the actual scenario.

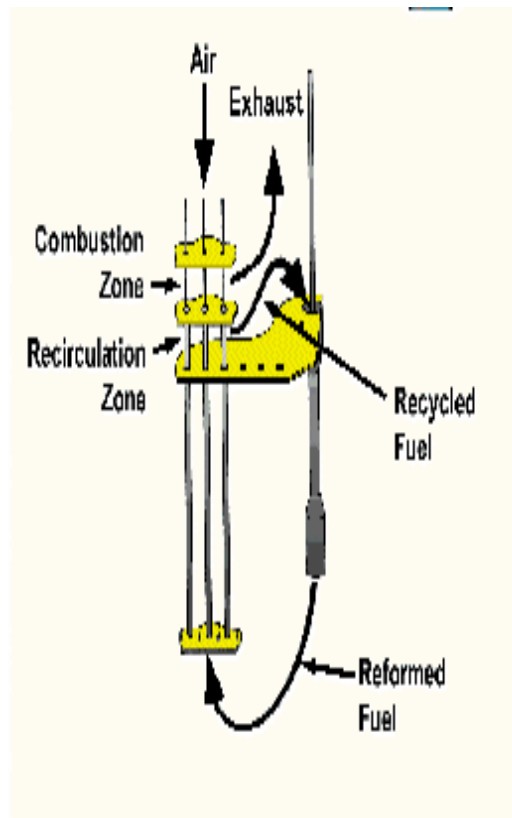


Figure 2.9: Recirculation scheme for indirect internal reformation (IIR)

Fig. 2.9 is a company schematic of the *recirculating-regenerative* mechanism by which SiemensWestinghouse TSOFC stacks internally reform fuel. Part of the anode exhaust recirculates to supply the necessary steam for safe reformation (i.e., a sufficiently high steam-to-carbon ratio in the fuel processing compartments to prevent coking). Radiation from the cells' exterior supplies the needed thermal energy to the reforming compartments. Cell stack operation thus supplies the needed heat *and* the needed steam for internal fuel processing.

Reconsider the definition for fuel utilization given in Eqn. (2.7). Fuel utilization is characterized by fuel flow rates at the cells' leading and tail edges; however, these flow rates do not represent the externally supplied and exhausted fuel flow rates. Specifically, recirculation results in the flow rate of externally supplied fuel being less than the fuel flow at the leading edges of the cells, and it causes the flow rate of fuel exiting the stack to be less than the flow rate of fuel at the cells' tail ends. Fuel utilization can thus become an arbitrarily chosen parameter. Depending upon whether one's interest is in the fuel cells' performance (as characterized in Eqn. (2.7)), or whether the interest is in externally fed fuel consumption (typical interest in *systems* design), fuel utilization will have differing meanings and values. While the present focus is upon SOFC technology, this ambiguity impacts other fuel cells designs as well (e.g., PEM fuel cell systems incorporating fuel stream recirculation).

Finally, the fuel utilization parameter is not a definitive indication of maximized fuel consumption within a cell stack. Ideally the limiting value for fuel utilization is 100%; however, this is not a practical limit since fuel cells are not typically intended for

“dead-ended” fuel supplies, wherein there is just enough fuel to support the current generated. Such an approach could lead to product integrity issues such as anode oxidation due to fuel starvation. Additionally, the *actual* limiting value for fuel utilization is that for which stream Nernst potential lowers to cell operating potential. Coupling this fact with the research emphasis upon increasing cell potential, *actual* fuel utilization limits may be significantly less than 100%. Thus, there is another point of uncertainty associated with fuel utilization in that the *theoretical* and *practical* limiting values for fuel utilization are different.

Electrochemical pinch points provide insights that are complementary to fuel utilization, yet without the associated ambiguities pointed out to the reader. Electrochemical pinch points allow one to evaluate cell performance based upon the conversion of chemical potential into electricity, as is the attempt of the fuel utilization parameter. An electrochemical pinch point is a state function, dependent upon anode-exit Nernst potential and cell potential (ref. Fig. 2.4b). Since it is not process- or path- dependent as is *electrochemical* fuel utilization, there is no ambiguity that arises from multiple paths by which CO may have been oxidized along the SOFC⁸. With respect to fuel stream flow management, electrochemical pinch points are again established for a specific location (fuel cell exit) and thus are insensitive in definition to whether fuel flow is single-pass or whether there is recirculation. Finally, an index-of-performance is more valuable when its limiting value corresponds to the limit of performance of the system being evaluated. For example, the thermal efficiency of a heat engine is limited by the Carnot efficiency constraint. The Carnot efficiency is typically much lower than 100%. Second law (or exergetic) efficiencies have thus been incorporated, wherein the maximum power possible of a heat engine is the point of evaluation instead of heat supply rate. The result is that ideal heat engine operation results in a maximum (i.e., 100%) second law efficiency, instead of a lower thermal efficiency that has an arbitrary appearance (e.g., 45% given a set of temperature limits). Electrochemical pinch points provide the same complement to fuel utilization. A fuel cell reaches its thermodynamic maximum performance when the electrochemical pinch point reaches the limiting case of zero. Physically, this is when the Nernst potential of the stream has lowered to the cell potential. The limiting case of zero is numerically more relevant and insightful than is a seemingly arbitrary fuel utilization limit that will be significantly less than 100%.

The concept of electrochemical pinch points is not proposed as a replacement for the critical decision variables operating voltage and fuel utilization, but it is shown to be a viable complement for cost-effective cell design and added clarity in the evaluation of fuel cell performance.

⁸ A counter-consideration, however, is that the electrochemical pinch point must be defined in a partially subjective manner; since the Nernst potential at the anode exit will need to be a weighted average of the Nernst potentials associated with hydrogen and carbon monoxide oxidation.

Tasks 3: Thermal-Fluid Modeling

The initial analysis on the monolith type SOFC was based on the geometry provided by NETL with the flow channels embedded within the electrodes of the fuel cell (Figure 3.1a). Most commonly found fuel stack geometries have the flow channels sandwiched between the positive electrode-electrolyte-negative electrode (PEN) structure and the interconnect plate (Figure 3.1b).

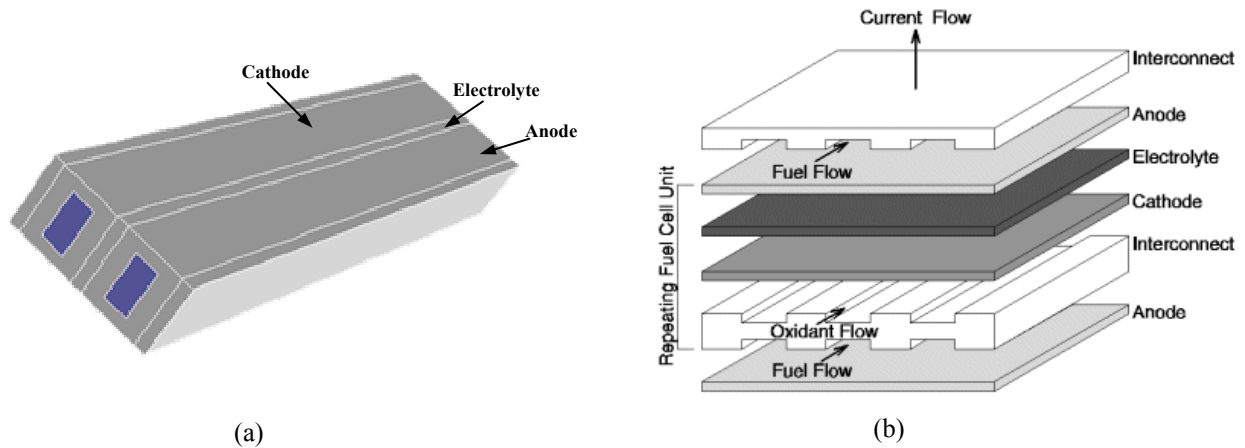


Figure 3.1: (a) Schematic of a single cell monolith type SOFC with the flow channels formed within the electrodes. (b) Schematic of a realistic SOFC cell modeled with the flow channels embedded between the PEN structure and the interconnect plates.

Figure 3.2 plots the temperature profiles along the centerline of the anode-electrolyte and the cathode-electrolyte interface for the initial monolith geometry and makes a comparison with the results obtained from the modified fuel cell configuration. The dimensions of the modified fuel cell and the boundary conditions used in the simulations are similar to those specified in the initial case study (see previous progress reports).

The presence of flow channels removed further away from the electrode-electrolyte interface results in an increased resistance to the flow and mass transfer within the electrodes. This accounts for the observed decrease in concentration of the reactant species along the interface, a decreased rate of the interfacial electrochemical reaction, and thus explaining the reduction in temperature within the modified monolith fuel cell geometry.

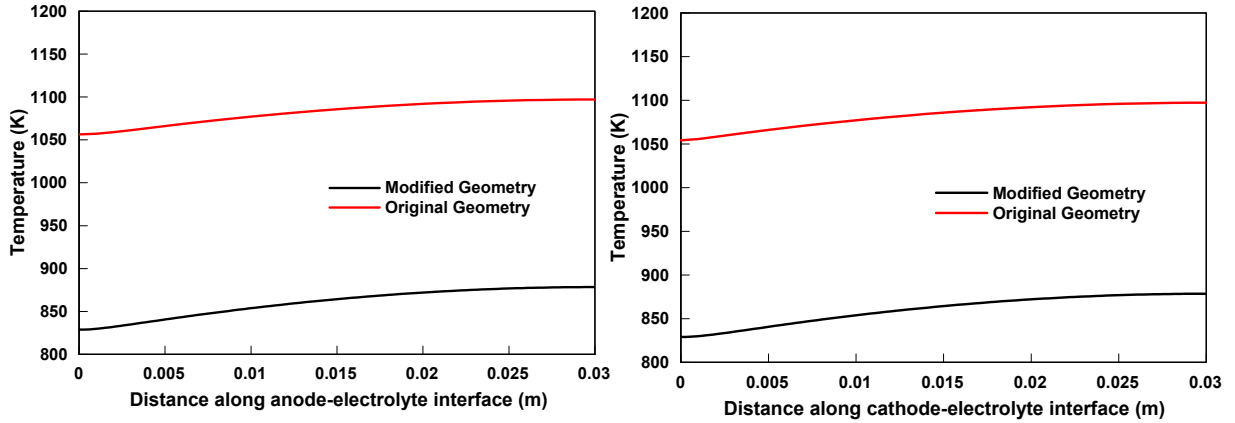


Figure 3.2: Temperature comparison along the anode-electrolyte and the cathode-electrolyte interfaces for the modified monolith fuel cell geometry with those obtained using the initial flow channel configuration.

The effect of radiation on the fuel cell temperature profile was also studied by solving the Radiative Transfer Equation (RTE) through the Discrete Ordinate Method (DOM) model in Fluent. The radiative properties of the electrodes and electrolyte are those obtained from the literature and have been described in detail elsewhere [3.1]. Inclusion of radiative transfer results in a 30 K drop in temperature within the fuel cell and is accompanied by a 2% increase in the cell voltage. Thus, the observed radiative heat transfer effects are reduced in magnitude in the case of more realistic SOFC geometry as compared to one originally used [3.1].

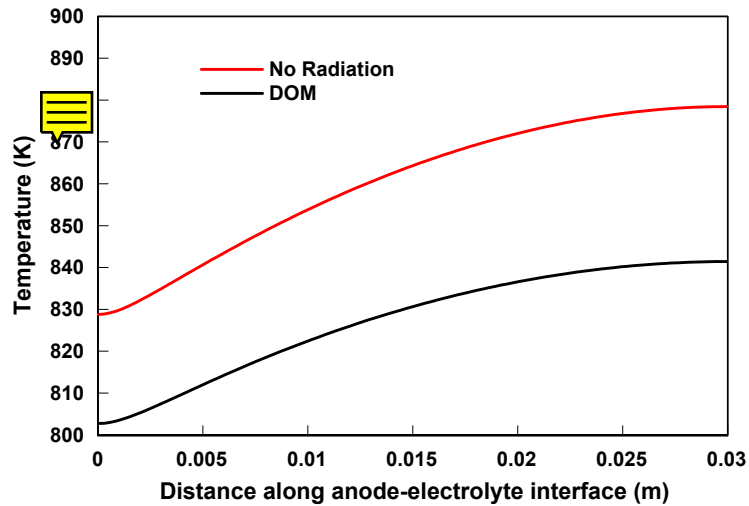


Figure 3.3: Temperature profiles along the anode-electrolyte interface obtained with and without inclusion of radiation effects in the fuel cell model

References:

[3.1] Murthy S. and Fedorov, A., “Radiation Heat Transfer Analysis of the Monolith Type Solid Oxide Fuel Cell”, *J. Power Sources*, in print.


Task 4: Multi-Physics Model Integration

Reduction in the feature dimensions of the electrodes and electrolyte results in rapid divergence of the numerical fuel cell model. Various known techniques in the area of under-relaxation and multi-grid modeling have proven to be unsuccessful in obtaining convergence. Current efforts are involved in establishing the root cause for the problem through a parametric study of the fuel cell variables.

Completed Tasks

Tasks 1.2, 1.4, 2.3, 3.1, 3.2, 3.3 are complete, all others are on going.

Key Milestone Update

Tasks	Status	Remarks
1.1 Obtain fracture mechanics parameters for cohesive, interfacial and impinging cracks.	90% complete 	
1.2 Model spalling phenomenon and thermal expansion induced stress during thermal transients and shock.	100% complete	
1.3 Identify and quantify crack path selection and crack propagation.	90% complete	
1.4 Implement temperature gradient as driving force for cracking. The Recipient shall investigate the individual and combined influences of electrochemical and mechanical load stress, as well as temperature gradients on crack initiation and propagation. The Recipient shall review and utilize/adapt, where appropriate, existing, available fracture mechanics models in order to advance the state-of-the-art.	100% complete	
1.5 Evaluate and validate the accuracy of developed fracture mechanics models using either experimental data or modeling results from PNNL/NETL/ORNL or other SECA members.	80% complete	
2.1 Utilize/adapt existing electrochemical models, and develop enhancements necessary to achieve the project objectives and to advance the state-of-the-art.	75% complete	
2.2 Models Extension to include porous electrode phenomena enhancements beyond the current state-of-the-art.	80% complete	
2.3 Evaluate and validate the accuracy of developed electrochemical models and enhancements using either experimental	100% complete	

data or modeling results from PNNL/NETL/ORNL or other SECA members.		
3.1 Formulation of 2-D and 3-D models for combined advection, conduction, and radiation heat and mass transfer in the porous electrodes.	100% complete	
3.2 Formulation of an approach for calculation of effective transport, thermophysical and radiative properties for the porous electrodes.	100% complete	I
3.3 Formulation of coupled heat/mass transfer and electrochemistry model on the "unit-cell" level. The Recipient shall account for boundary effects, such as oxidant and fuel flow field channels, electrical interconnects and seals.	100% complete	.
3.4 Review, select, and develop solution algorithms for numerical solution.	80% complete	
3.5 Evaluate and validate the accuracy of developed thermal models, algorithms and enhancements using either experimental data or modeling results from PNNL/NETL/ORNL or other SECA members.	80% complete	
4.1 Review the implementation strategy of developed modeling modules within the PNNL/NETL simulation platform.	50% complete	
4.2 Assess and identify areas within the PNNL/NETL simulation platforms where improvements will advance the state-of-the-art and contribute to the overall SECA Modeling and Simulation Program.	100% complete	

Discussion Topics

The following issue has not been resolved. The Georgia Tech academic license for ANSYS allows only very limited number of nodes in the analysis. As we are moving into analyzing more realistic cell stacks, a full functional version of ANSYS will be needed. One possible solution to this problem is to obtain an account in NETL or PNNL computers where the full functional ANSYS is available. We can then run the program on the NETL/PNNL computer via the internet. This is becoming a critical issue that needs immediate attention.

Significant Accomplishments

- Developed a model to simulate thermal cycling induced failure during steady-state operation.

- Analogs has been established between fuel cells and heat exchangers. The end-goal is to glean principles from the mature areas of heat exchanger design and characterization into similar areas within the maturing field of fuel cells simulation. Focused attention is given to the concept of electrochemical pinch points as a supplement to traditional fuel cell parameters.
- Studied the effect of radiation on the temperature fields of the modified, more realistic monolith SOFC geometry.

Science & Technology Transfer

None to report

Presentations & Publications

None to report

Site Visits

None to report

Travel

J. Qu attended the Seal Workshop in Albuquerque.

APPENDIX

Calculation of the convection coefficient involves determination of several dimensionless parameters. The first one is the Nusselt number (A.1), which is a dimensionless form of the local convection coefficient given by

$$Nu = \frac{hx}{k} \quad (A.1)$$

where,

Nu = Nusselt number
 h = convection heat transfer coefficient
 k = thermal conductivity of air
 x = local distance along plate

For laminar flow along a flat plate the local Nusselt number in the x-direction can be related to the Reynolds (Re_x) and Prandtl (Pr) numbers with equation A.2. (assuming constant wall temperature boundary condition)

$$Nu_x = 0.343 Re_x^{1/2} Pr^{1/3} \quad (A.2)$$

where the Reynold's number can be calculated as follows:

$$Re_x = \frac{\rho V_\infty x}{\mu} \quad \text{where,}$$

ρ = density of air
 V_∞ = flow velocity of air
 μ = viscosity of air

(A.3)

The thermophysical properties used to calculate the Nusselt number and the convection heat transfer coefficient are temperature dependant properties of air. However, for the temperature ranges used for the analysis the effect of varying temperature on the final convection coefficient was found to be minimal. Because of this the following constant property values were used in all calculations of the convection coefficient.

$$\begin{aligned}
k_{air} &= 65 \times 10^{-3} \frac{\text{W}}{\text{mK}} \\
\rho_{air} &= 0.35 \frac{\text{kg}}{\text{m}^3} \\
\mu_{air} &= 425 \times 10^{-7} \text{ Pa} \cdot \text{s} \\
\text{Pr}_{air} &= 0.72 \text{ dimensionless}
\end{aligned}
\tag{A.4}$$

All values are taken at 1000°K

After calculating the Nusselt number as a function of distance along the x-axis the convection heat transfer coefficient was calculated by rearranging equation A.1. The behavior of the convection coefficient along x is shown in the curves of Figure A.1.

$$h(x) = \frac{Nu_x k}{x} \tag{A.5}$$

As expected, at the leading edge the heat transfer coefficient is singular and approaches infinity because of infinitesimally thin thickness of the thermal boundary layer.

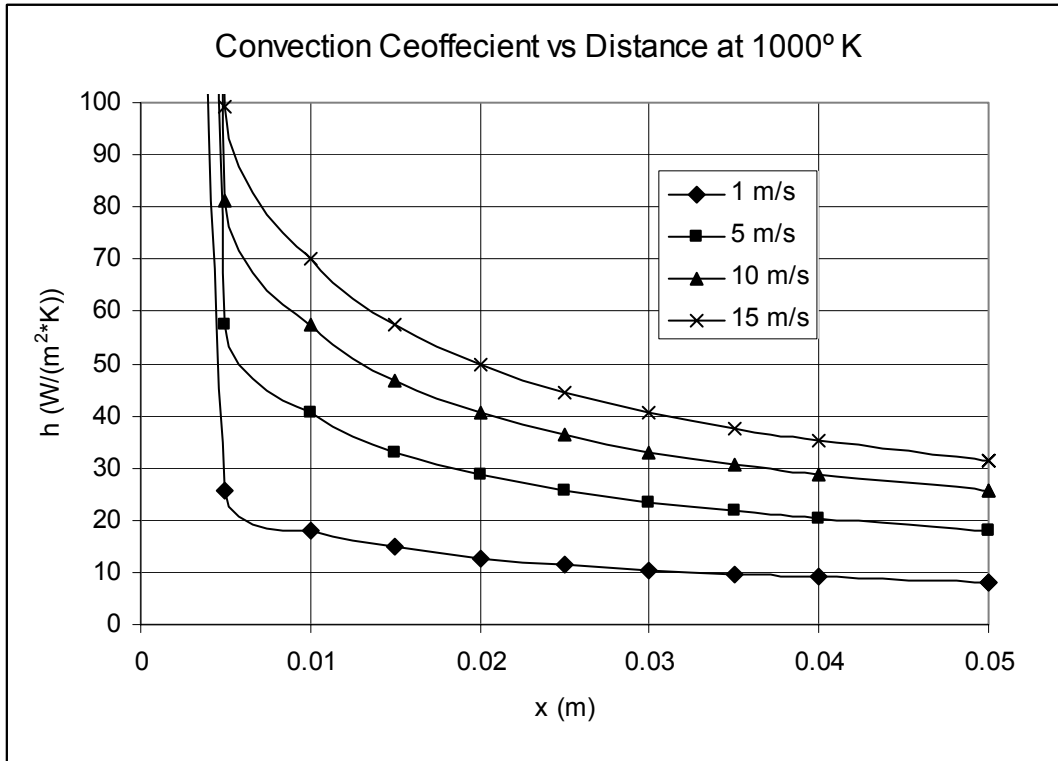


Figure A.1: Variation of Convective Heat Transfer Coefficient